Control Strategies for Multi-Rotor Wind Turbines

Finn Matras[1] and Morten Dinhoff Pedersen[1]

[1]Department of Engineering Cybernetics, Norwegian University of Science and Technology, Trondheim, Norway

Correspondence: Finn Matras (finn.matras@ntnu.no)

Abstract. This work considers steady-state aspects of multi-rotor wind turbine control. In contrast to most literature on the topic, the underlying multi-rotor model includes the aerodynamic interactions between the rotors. The model predicts that these interactions are central for effective control of multi-rotor wind turbines under some conditions. A numerical optimization problem is formulated to find the optimal control solutions, and two adaptations of the MPPT algorithm for the multi-rotor case are suggested. By employing furling for multi-rotor wind turbines, it is also shown that one can drastically reduce the bending moment of the structure. Other physical effects such as operation with wind shear and simple failure handling are also presented using a 23-rotor fixed-pitch multi-rotor wind turbine with a total rated power of 5 MW. The results are meant as an enabling work, showcasing the possibilities and challenges involved in multi-rotor stability analysis and control problems.

1 Introduction

This work is a compilation of the relevant work for multi-rotor wind turbines presented in the thesis of the main author Matras (2025).

Multi-Rotor wind turbines have been a known concept for several centuries, but they have almost been disregarded when compared to their single rotor counterparts. In a quest for cost reduction, the single-rotor wind turbines have become bigger and bigger. While there might be many reasons for this trend, the scaling laws dictate structural and aerodynamic challenges due to increasing rotor sizes. A natural alternative to increasing the rotor radius is to increase the rotor count, and possibly to work with, rather than against, the scaling laws by reducing the rotor radius. The idea has been investigated by reputable industry companies such as Vestas van der Laan et al. (2019) and recent startups such as Wind Catching Systems AS (2021) and Myriad Wind Energy Systems (2024).

The multi-rotor concept with smaller rotor radii has many advantages, mainly rooted in the fact that it can be considered to discretize the continuous wind field in smaller areas, allowing it to more efficiently utilize the spatially varying wind field. Authors such as Jamieson (2011); Jamieson and Branney (2014); Sandhu (2018) have investigated and discussed other aspects of rotor scaling and multi-rotor setups.

Successful application of multi-rotor wind turbines requires a thorough understanding of the system behavior and how they are best controlled for maximal power generation, load reduction and stability. The available literature on the topic is somewhat sparse, which is highlighted by the control challenge proposed in Sørensen et al. (2018), motivating researchers to contribute to the topic. Spagnolo et al. (2020) responded to the challenge and developed an extremum-seeking controller. Other

aspects such as yawing of a two-rotor wind turbine with variable pitch and optimal differential thrusting was investigated by Guenoune et al. (2016) and MacMahon and Leithead (2018), respectively. Unfortunately, none of these contributions include the aerodynamic interactions between the rotors, which is believed to be significant based on their significance for multi-rotor helicopters Johnson (1994). Additionally, a multi-rotor setup with many smaller rotors will be able to better adapt to the local flow conditions than an equivalently big single rotor system. Thus, a multi-rotor can sample the wind field with greater fidelity than a single rotor system. This sampling gives rise to further interactions that are assumed to be of importance. The present work will include a simplified model of the interactions, allowing an investigation of how they affect the control and stability of a multi-rotor wind turbine at steady-state in the various operating regimes. The knowledge obtained from the analysis can be used to guide future attention to the areas that are of significance for multi-rotor systems.

Modeling and control of single rotor wind turbines is relatively well described in the literature, see Manwell et al. (2010); Apata and Oyedokun (2020); Barzegar-Kalashani et al. (2023). The majority of large single rotor wind turbines have blades with variable pitch, which adds modeling, design and control complexity, as well as increasing the number of failure points. Another advantage of multi-rotor wind turbines with smaller rotors is their increased rigidity which can allow for control techniques using stalling or furling to effectively achieve a similar level of power control as a variable pitch turbine. Furling for a multi-rotor wind turbine can be achieved by rotating the whole support structure to produce a yaw offset as indicated by ψ in Fig. 1. This technique will be used to illustrate an intriguing operation scheme for when the multi-rotor wind turbine needs to limit its power output.

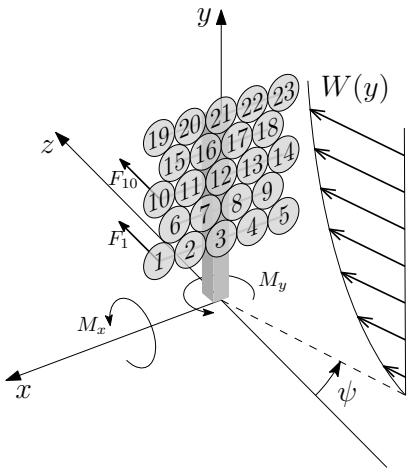

Figure 1. Illustration of turbine configuration, the x, y and z coordinates, ambient wind speed $W(y)$ and direction ψ, thrusts F and torques M.

2 Overview

As established in Matras and Pedersen (2024), the dynamics of multi-rotor systems are influenced by both the rotor count and the size of each individual rotor. This complicates any general study on the topic by making results case dependent, but it can be omitted by discussing overall system behavior at steady-state, which is what will be done in this work.

From a control perspective one can identify two main modes of operation at steady-state: unconstrained and constrained operation. The former case considers the phase in which the main goal of a wind turbine is to maximize its energy production. This is typically achieved by using the well-known Maximum Power Point Tracking (MPPT) controller that dictates a generator torque proportional to the rotational velocity squared, as discussed in Johnson et al. (2006). While this has proven to work well for single-rotor turbines, its efficacy for the multi-rotor case has still to be proven. To this end, the results from applying the MPPT algorithm to each individual turbine is compared to the numerically optimal solution.

The second mode of operation, the constrained mode, can be trickier to handle due to the system complexity and the varying nature of the constraints. Algorithmically, this complicates the design because the MPPT algorithm is no longer viable, and other controllers need to be developed. The present work will consider the numerically optimal solution, even though this can be too complex for real-time control. An advantage of the numerical optimal solution is that the solutions relatively easily can be computed for any desired constraints, of which the individual power constraint, a net bending moment constraint and yaw moment constraints are considered here to highlight some interesting properties of multi-rotor systems.

The findings from the two modes of operation are then used to inform a novel control strategy for multi-rotor wind turbines that by definition of Skogestad and Postlethwaite (2005) is self-optimizing, thus operating close to the numerically optimal solution using inherent system properties. It is worth noting that also this analysis only considers the steady-state behavior and substantial engineering efforts still need to be made to get a proficient dynamic control system.

3 Modeling

The foundation of the analysis is a simple steady-state multi-rotor model presented in Matras et al. (2024) based on the actuator disk concept. The main novelty of this model comes from the inclusion of the aerodynamic interactions between the rotors. Wind shear is also included as an extension of the model presented in Matras et al. (2024), and the required model parameters are adjusted to fit a 23-rotor wind turbine as shown in Fig. 1. Taking inspiration from the NREL 5 MW reference turbine from Jonkman et al. (2009), the net rated power of 5 MW, and total swept area, is divided equally among all the turbines and the center of the tightly packed multi-rotor turbine coincides with the hub height of the NREL 5 MW reference turbine. Additionally, the rotors are set to have pairwise opposing rotational directions so that the axial torques cancel out. The blockage effect as evaluated in McTavish et al. (2015) is not included, as this would require a more complex model.

Following Matras et al. (2024), the model is decomposed as originally proposed in Joglekar and Loewy (1970) as shown in Fig. 2. The decomposition allows for a clear separation of the various submodules, so that each can be modeled independently. The main input to the model, which is also the source of energy, is the freestream wind of strength $W(y)$ with direction ψ. Combining the freestream wind, the rotation of the rotors $\boldsymbol{\omega}$ and the axial induced flows of all rotors $\boldsymbol{v}$ produces a relative

velocity over the rotor blades which are mapped to forces through the airloads module. These forces are then fed back into the mechanics and inflow modules to compute the resulting mechanical and flow perturbations. The feedback structure gives and intuitive understanding of the system behavior, and also allows to implement the multi-rotor interactions by extending the inflow and mechanical modules, while the remaining modules remain decoupled on the rotor level.

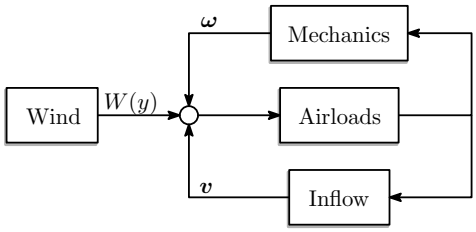

Figure 2. Block diagram of system submodules.

In the following, it is assumed that three critical measurements are available for each of the turbines $n \in [1, N]$, namely the electrical power P_n, the rotational velocity ω_n and the thrust F_n. With these three measurements, it is possible to estimate the required quantities for control purposes, as will be discussed later. The electrical power is assumed to be measured at the output with good estimates for the losses, such as the drivetrain and generator losses, so that the shaft power can be determined. The rotational velocity is assumed to be an accurate direct measurement from, for instance, a hall sensor. Finally, the thrust is also assumed to be a directly measurable quantity using a pressure plate between the thrust bearing and the support structure. Sideways forces are excluded for model simplicity, and as shown in Matras et al. (2023), these are often two orders of magnitude smaller than the axial forces.

3.1 Induced Flows

The model developed in Matras et al. (2024) can be seen as a special case of the input coupling inflow model Matras (2025). It describes the relation between a column vector of mean thrust $\boldsymbol{f}$ and a column vector of mean axial flows $\boldsymbol{v}$. The relation is found as

$$\boldsymbol{v} = \mathbf{A}\boldsymbol{f}. \tag{1}$$

The matrix $\mathbf{A}$ describes the relation between the forces and flows, and depends on the rotor layout and the skew angle. Figure 3 illustrates how the pressure forcing of two rotors is converted into a flow using the $\mathbf{A}$-matrix.

The simplest case, where all rotors are spaced sufficiently apart so that they can be considered isolated from one another yields a diagonal matrix. Moving the rotors closer together adds interactions which become visible on the off-diagonals. To include a skewed flow with average skew angle χ, the matrix $\mathbf{A}$ requires an expansion in $\tan(\chi/2)$ to be computed

$$\mathbf{A} = \sum_{m=0}^{M-1} \mathbf{A}_m \tan(\chi/2)^m. \tag{2}$$

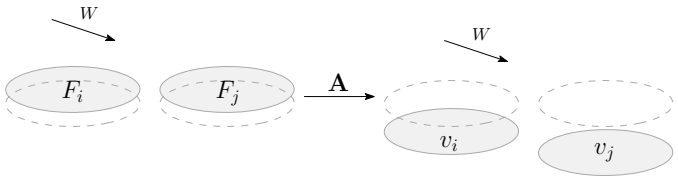

Figure 3. Illustration of inflow model with skewed flow.

As illustrated in Fig. 4, the skew angle is defined as the angle between the axial unit vector and the net flow that passes through the rotor. The simplified model uses a global skew angle, computed on the average wind speeds of all rotors. While this can be seen as a somewhat crude approximation, it is believed to be suitable for the simplified analysis presented in this work.

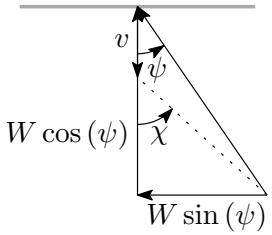

Figure 4. Illustration of induced velocity and the related angles.

A normalized example of the two first terms of the expansion of $\mathbf{A}$ for four rotors placed in a tightly packed square are

$$\bar{\mathbf{A}}_0 = \begin{bmatrix} 1 & 0 & 0 & 0 \\ 0 & 1 & 0 & 0 \\ 0 & 0 & 1 & 0 \\ 0 & 0 & 0 & 1 \end{bmatrix}, \quad \bar{\mathbf{A}}_1 = \begin{bmatrix} 0 & -0.26 & -0.08 & 0 \\ 0.26 & 0 & 0 & 0.08 \\ 0.08 & 0 & 0 & 0.26 \\ 0 & -0.08 & -0.26 & 0 \end{bmatrix}. \tag{3}$$

It is clear that the zeroth term, representing the self influence, is constant regardless of the skew angle. The first term is skew-symmetric and represents the linear, in $\tan(\chi/2)$, interactions between the rotors. A few more terms are needed for good coverage of higher skew angles, so the remainder of this work includes 10 terms for the modeled multi-rotor.

3.2 Rotor Airloads

In accordance with the rest of the model, the airloads will also only consider mean axial linear and rotational velocities as inputs, generating axial linear and rotational forces, F and q, respectively. The modeling of the airloads is further simplified by using dimensionless inputs and outputs. The input is considered to be a slightly modified Tip Speed Ratio (TSR) given by

$$\hat{\lambda} = \frac{\omega R}{w}, \tag{4}$$

where the $w = W\cos(\psi) - v$ represents the net axial flow through the rotor, and not only the freestream component as in the typical definition of the TSR. The fixed-pitch rotor model only takes this TSR as input. At the optimum, where momentum theory predicts $v = \frac{W\cos\psi}{3}$, the modified TSR becomes $3/2$ times the traditional TSR.

Similarly, the outputs are also made dimensionless by using the thrust coefficient

$$C_T = \frac{F}{1/2\rho\pi R^2 (W\cos(\psi))^2} \tag{5}$$

and torque coefficient

$$C_Q = \kappa \frac{q}{1/2\rho\pi R^3 (W\cos(\psi))^2}, \tag{6}$$

scaled by $\kappa = 10$ to make it of similar magnitude as the thrust coefficient. Here, ρ describes the fluid density and R the rotor radius.

Using the approach from Matras et al. (2023), the input-output relation for the airloads was found using the Blade Element Method (BEM) for $\hat{\lambda} \in [0, 30]$ using the data presented in Jonkman et al. (2009). The dimensionless model then makes it possible to scale the relation to the desired rotor size. Continuing as in Matras et al. (2023), the BEM data is then used to train a neural network implemented in Flux Innes et al. (2018); Innes (2018) using the AdaBelief Zhuang et al. (2020) backpropagation algorithm in Julia Bezanson et al. (2017). Thorough tuning of model dimensions, activation functions, weights and biases revealed the model shown in Fig. 5, where the blue square represents the input, the blue circles represent neurons, the thickness of the lines represents the weight of the connections and the red dots the bias. The activation function for the two hidden layers is the `tanh` function, and the output layer uses a unitary activation function.

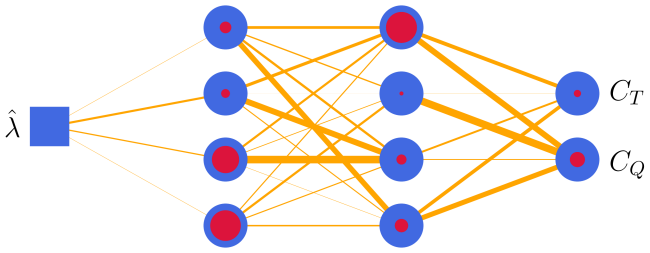

Figure 5. Illustration of the neural network, weights in orange, bias in red.

Mathematically, the artificial neural network with weights $\mathbf{W}$ and biases $\boldsymbol{b}$ is given by

$$\begin{bmatrix} C_T \\ C_Q \end{bmatrix} = \mathbf{W}_3 \tanh\left(\mathbf{W}_2 \tanh\left(\mathbf{W}_1 \hat{\lambda} + \boldsymbol{b}_1\right) + \boldsymbol{b}_2\right) + \boldsymbol{b}_3. \tag{7}$$

As expected from the results presented in Matras et al. (2023), the performance is excellent as shown in Fig. 6.

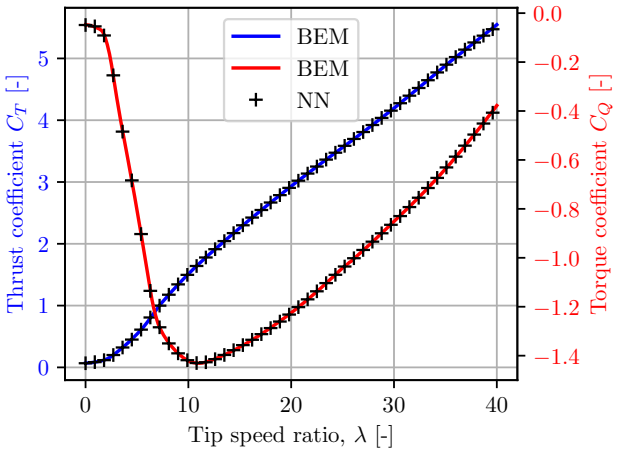

Figure 6. BEM results compared to the neural network (NN).

3.3 Mechanics

Only the fundamental mechanics required to represent a multi-rotor system at steady-state will be considered here. These are the yaw moment and the net bending moment around the base

$$M_y = \sum_{n=1}^{23} F_n x_n, \tag{8}$$

$$M_x = \sum_{n=1}^{23} F_n y_n, \tag{9}$$

where x_n and y_n are the x and y positions of rotor n. The steady-state nature of the model allows the rotational velocity of rotor n, ω_n, to be set directly as the appropriate torque will be produced by the generator to maintain steady-state,

$$q_{g,n} = -q_n \tag{10}$$

3.4 Wind

The final block in Fig. 2 that needs to be modeled is the wind. Assuming a horizontally constant freestream field of strength $W(y)$ and direction ψ, one only needs to model the wind shear. This endeavor has been undertaken many times previously, so the well known power law profile presented in Manwell et al. (2010) is used,

$$W(y) = W_r \left(\frac{y}{y_r} \right)^{\alpha}. \tag{11}$$

The reference velocity W_r at height $y_r = 2$ m, is scaled to height y, and the relation can be adapted to any particular site by adjusting α. Following Schlichting and Shapiro (1968), we use $\alpha = 1/7$.

4 Unconstrained Operation

This section will investigate the unconstrained operation of a multi-rotor wind turbine that maximizes the produced power.

4.1 Control Law

The MPPT algorithm is an excellent candidate for controlling a single rotor wind turbine in the unconstrained region, Abdullah et al. (2012). By considering the steady-state operation around the optimum, taking only the rotational velocity as a variable, an optimal and stable solution for the generator torque is found as

$$q_{g,n} = \frac{1}{2}\rho\pi R^2 C_p^* \left(\frac{R}{\lambda^*}\right)^3 |\omega_n|\omega_n. \tag{12}$$

The optimal power coefficient C_p^* and the corresponding traditional TSR λ^* have to be computed beforehand. When applying the MPPT algorithm to each individual turbine in a multi-rotor wind turbine without considering the interactions this will be called Distributed Maximum Power Point Tracking (DMPPT).

During strictly axial flows, the DMPPT algorithm is equivalent to solving the optimization problem

$$\max_{\boldsymbol{\omega}} \sum_{n=1}^{23} -\omega_n q_n \quad \text{s.t. model equations} \tag{13}$$

for the simple model considered in this work. This optimization problem was implemented in Julia Bezanson et al. (2017) using the JuMP Dunning et al. (2017) package and solved using the IPOPT solver Wächter and Biegler (2006).

4.2 Operation Characteristics

At steady-state without constraints it is optimal for the multi-rotor to be aligned with the wind. The inflow model predicts no interactions in this case, making the DMPPT optimal. This is indeed verified by comparing the results from the DMPPT to the numerically optimal solution by solving (13).

Figure 7 and Fig. 8 show the powers and thrusts for the unconstrained case with an ambient wind speed of 9 ms^{-1} at the array center. The effect of the wind shear is clear, as both the thrust and power increase with height.

4.3 Yaw Moment

As long as the individual wind turbines can be considered decoupled, the analysis is straight forward as it strongly resembles a gathering of single rotor systems, which are described in the literature. However, once the aerodynamic interactions come into play, this changes. In an effort to analyze these interactions, they are provoked by enforcing a yaw offset, which in turn generates horizontally varying operating conditions across the array. These changes will in turn result in varying thrust distributions affecting the horizontal stability of the multi-rotor wind turbine.

Consider the case in which the multi-rotor wind turbine is not aligned with the flow. Now, the side that is closest to the wind, the upwind side, extracts energy from the wind, reducing the axial wind speed. Because the multi-rotor is not aligned with the

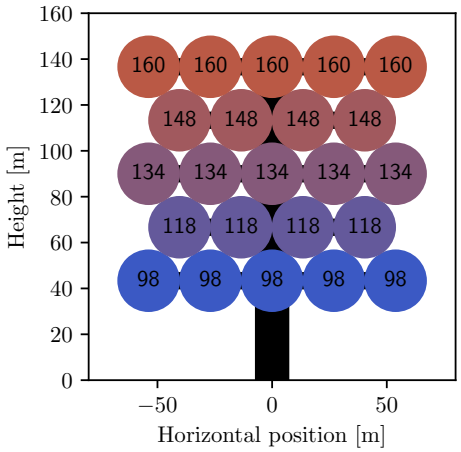

Figure 7. Powers in kW of multi-rotor wind turbine in wind shear with 9 ms^{-1} wind velocity at array center.

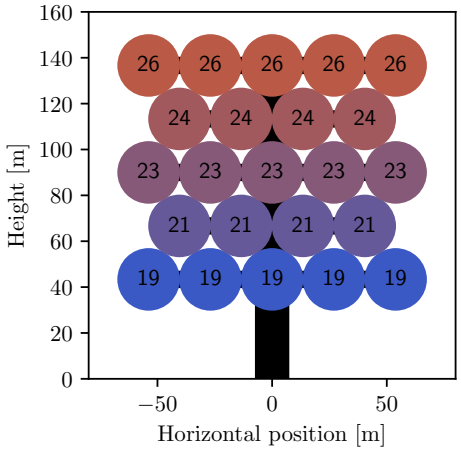

Figure 8. Thrusts in kN of multi-rotor wind turbine in wind shear with 9 ms^{-1} wind velocity at array center.

flow, this means that some component of this slightly perturbed, slowed down, part of the flow, will traverse onto the downwind turbines. This effect multiplies itself the further downwind one travels on the multi-rotor. Figure 9 illustrates the mean net axial flow through each rotor with a 45° yaw misalignment. The upwind side is to the right in the figure and the interactions can be clearly seen.

When operating in the unconstrained region, in which the thrust correlates with the ambient wind speed, this means that the thrust also decreases downwind. Fortunately, this effect produces a restoring moment which tries to realign the multi-rotor with the wind as shown in Fig. 10. At the peaks, the restoring moment is approximately equivalent to moving the center of thrust by

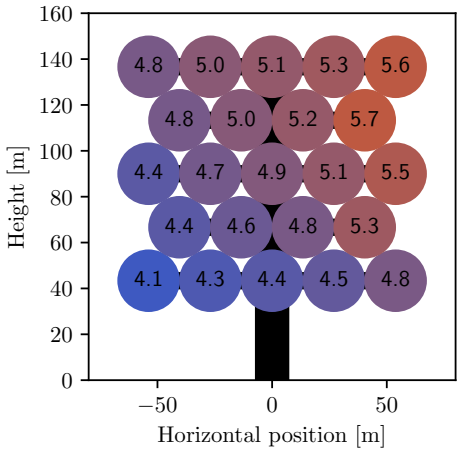

Figure 9. Mean axial wind speed ($W\cos\psi - v$) in ms^{-1} with 45° yaw misalignment.

3 m, slightly more than 2% of the multirotor width, upwind. A torque of similar magnitude can be obtained by turning off one of the upper and outermost rotors when the wind-turbine is aligned with the wind.

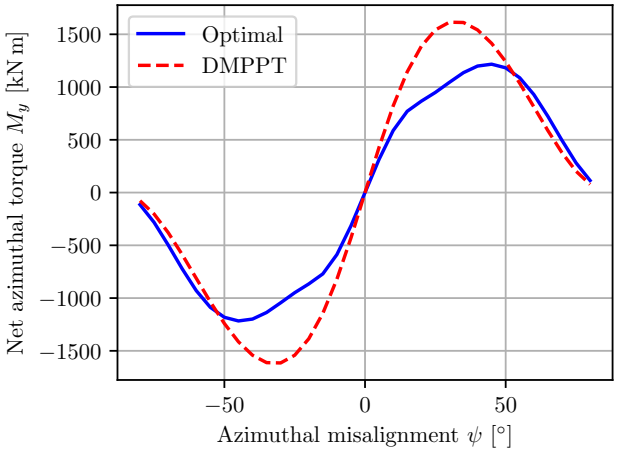

Figure 10. Influence of yaw misalignment on yaw moment.

The interactions also cause a reduction in total power, which increases with increasing skew angle as shown in Fig. 11. Both figures show the results obtained with the DMPPT algorithm and with the numerically optimal solution. While the general characteristics are the same, there are some differences. Mainly, the optimal solution is able to leverage the interactions to increase the total power by a maximum of about 2 % of the rated power, compared to the DMPPT algorithm that tries to maximize the power for each rotor independently. The leveraging of the interactions also has the effect of reducing the yaw

moment drastically for intermediate misalignments, as the optimal solution is to reduce the power on the upwind rotors so that the wind has more kinetic energy available for the downwind rotors. This results in a more even thrust distribution, which drastically affects the yaw moment because the thrusts are weighted by the horizontal distances to the center of the wind turbine.

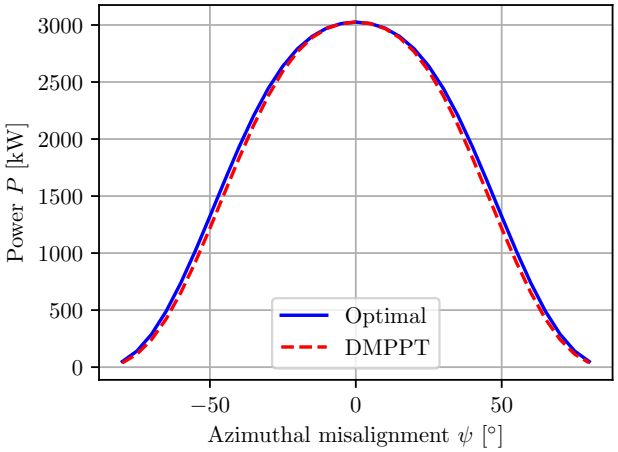

Figure 11. Influence of yaw misalignment on the total power.

The restoring moment is necessary, but not sufficient to determine if the multi-rotor is at a stable equilibrium when it is aligned with the wind. In addition to the restoring moment, one would also need to consider the dynamics of the total system to form a sufficient argument. However, it is believed that with the appropriate utilization of dampers the equilibrium can be made stable if it is not already. The damping effect could be implemented either physically, or digitally using differential thrusting. Differential thrusting can be achieved by manipulating the generator torques so that the corresponding rotors change their thrusts, effectively manipulating the net yaw moment. In this sense, the differential application of generator torques can be seen as a proxy for a yaw actuator.

When the stability of the system is ensured, one can conclude that the DMPPT algorithm exhibits a variation of self-optimizing control, Skogestad and Postlethwaite (2005), that will always try to realign the multi-rotor with the freestream wind.

5 Constrained Operation

The second and maybe more interesting operating region is the constrained region in which various physical constraints need to be respected. In contrast to a single rotor, the multi-rotor has constraints both on the rotor level, such as maximal power or thrust, and on the multi-rotor level such as the net yaw moment and bending moment.

5.1 Control Law

The DMPPT algorithm is no longer valid in the constrained case, and the general numerical optimal solution presented in (13) needs to be expanded to include constraints

$$\max_{\boldsymbol{\omega}} \sum_{n=1}^{23} -\omega_n q_n - Q \sum_{n=1}^{23} F_n y_n \tag{14}$$

s.t.

model equations

$$-\omega_n q_n \leq P_{max} \; \forall \; n \tag{15}$$

$$\psi = \psi^*, \text{ (optional)} \tag{16}$$

$$M_y = 0, \text{ (optional)} \tag{17}$$

$$M_x \leq B_{max}, \text{ (optional)}. \tag{18}$$

The star symbol is used to denote a reference value. A small penalty for the bending moment, with $Q = 5 \times 10^{-10}$, is added to guide the solution towards the optimum that also reduces the bending moment without significantly influencing the power, the importance of this will be shown later.

5.2 Individual Power Constraints

Figure 12 through Fig. 17 show varying characteristics of the multi-rotor, when aligned with the wind, found at the solution to (14) with the power constraints on each individual turbine from (15).

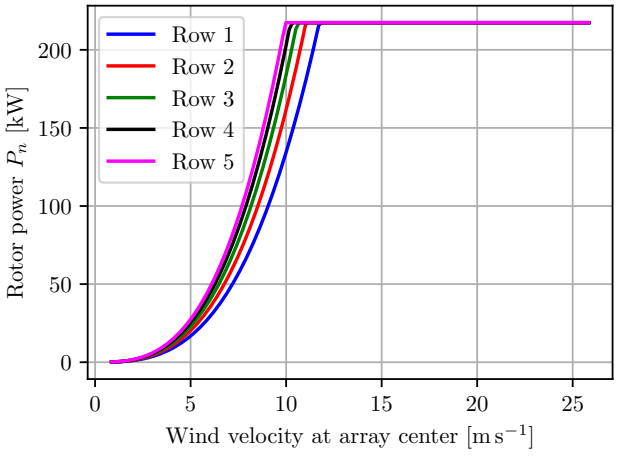

Figure 12. Power per rotor in each row with individual power constraints.

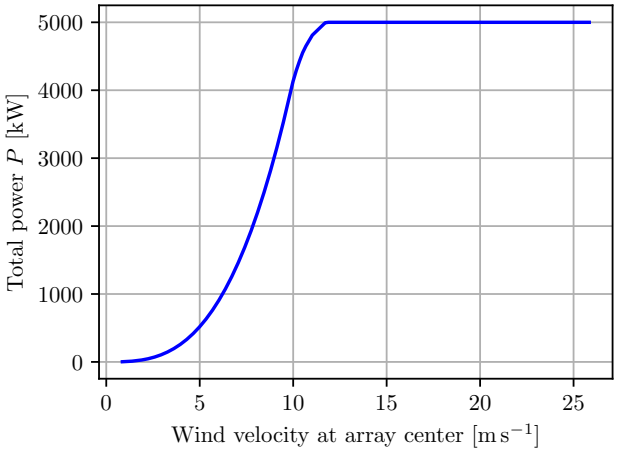

Figure 13. Total power with individual power constraints.

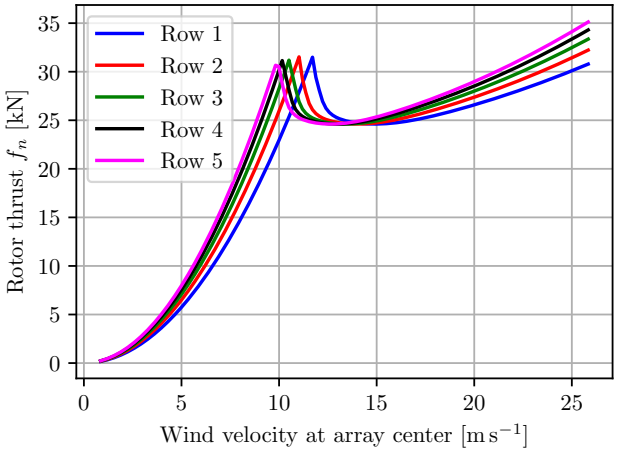

Figure 14. Thrust per rotor in each row with individual power constraints.

The effect from the wind shear is clearly visible, affecting each row of the multi-rotor differently. Intuitively, the top row of rotors, row 5, reaches the power constraint first as shown in Fig. 12, while the remaining rows follow in order. An advantageous consequence of this is that the total generated power shown in Fig. 13 has a smoother transition from the unconstrained to the constrained region. The same effect is visible for the thrusts in Fig. 14 and Fig. 15.

230 Interpreting the above findings, one could conclude that the rotors in one row could advantageously differ from the rotors in the other rows. For instance, the upper rotors should be optimized and rated for higher wind velocities than the lower rotors.

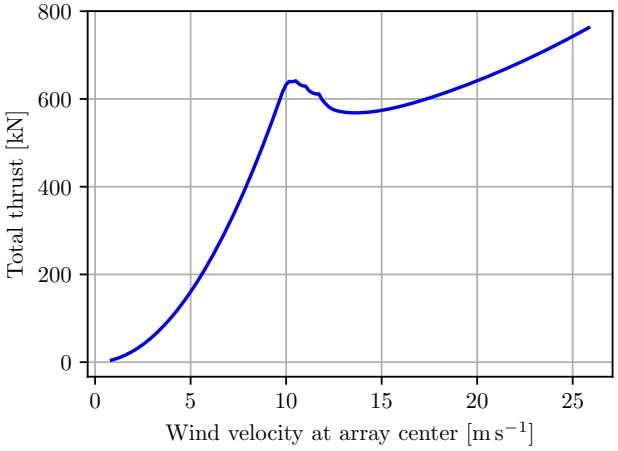

Figure 15. Total thrust with individual power constraints.

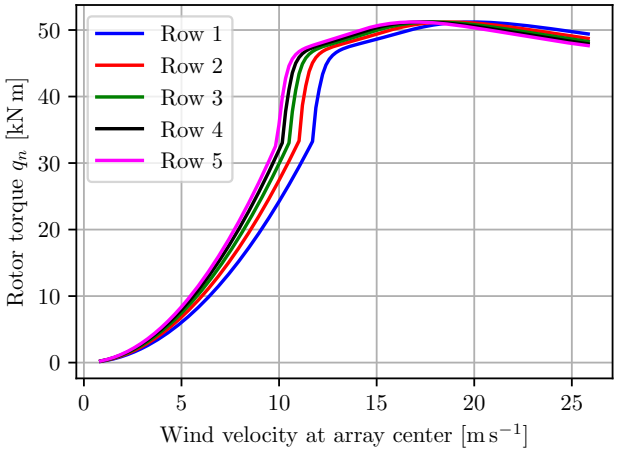

Figure 16. Torque per rotor in each row with individual power constraints.

Such an adjustment could increase the total generated power, but consequently also the loads on the support structure. This would also reduce the smoothing behavior seen when each row hits the constraint at slightly different velocities.

Figure 17 shows the advantage of including the small penalty on the bending moment in (14), because once the fixed-pitch rotor reaches the rated power, it can decrease the power by either increasing or decreasing the TSR as shown in Fig 6. Increasing the TSR would further increase the thrust, which is not desired, so the other solution found by decreasing the TSR is sought and found as can be seen in Fig. 17 and Fig. 14.

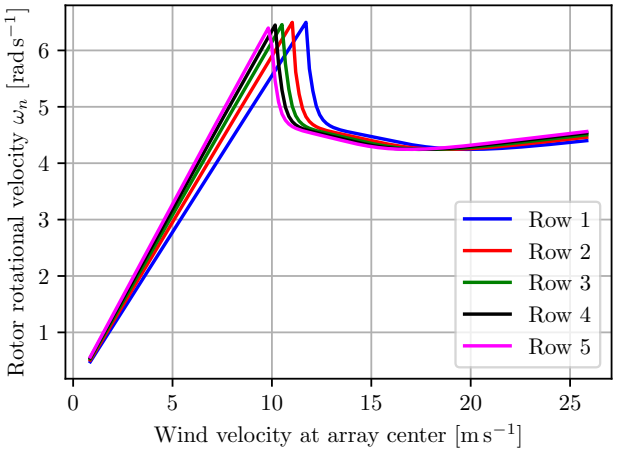

Figure 17. Rotational velocity per rotor in each row with individual power constraints.

5.3 Net Bending Moment Constraint

In addition to placing constraints on the generated power to protect the drivetrain, generator and power electronics, a net bending moment constraint can also be added to protect the support structure. The net bending moment constraint for a multi-rotor can be seen as a weighted equivalent to the thrust constraint for a single rotor. Comparing the total thrusts from Fig. 15 to the unconstrained net bending moment in Fig. 18 one can clearly see the resemblance between the two values, but the net bending moment puts a higher weight on the rotors that are placed higher, because they increase the loading on the structure more.

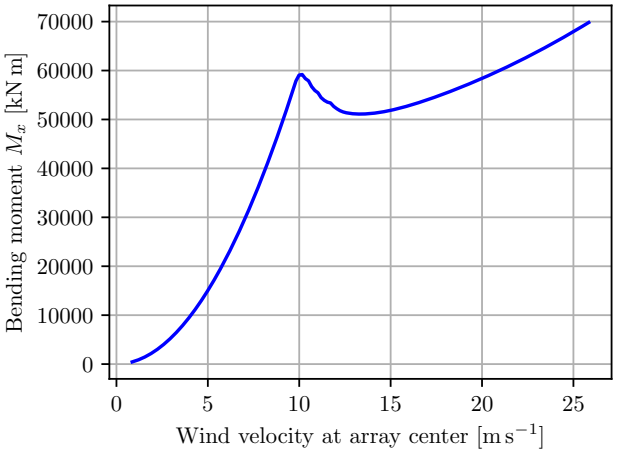

Figure 18. Net bending moment.

One can easily include the net bending moment constraint (18) with $B_{max} = 5 \times 10^7$ Nm in the optimization problem. The solution to (14) with (15) and (18) for a wind velocity of 17 ms^{-1} at the center of the array produces an allocation that result in powers and thrusts as shown in Fig. 19 and Fig. 20, respectively. As can be seen, most rotors operate at the power constraint, and only the top rotors have started reducing thrusts by slowing down the rotors starting from the middle and going outwards. The top rotors are turned off first, because they have the greatest impact on the bending moment. This results in a total power reduction of 8 %. The relation between power and thrust in the current case, where power is limited by reducing the TSR, enforces an L1 penalty on the system, favoring sparsity rather than reducing the power equally on all rotors.

In the presence of pitch-control, this issue is typically mitigated by pitching the blades, so no power is lost.

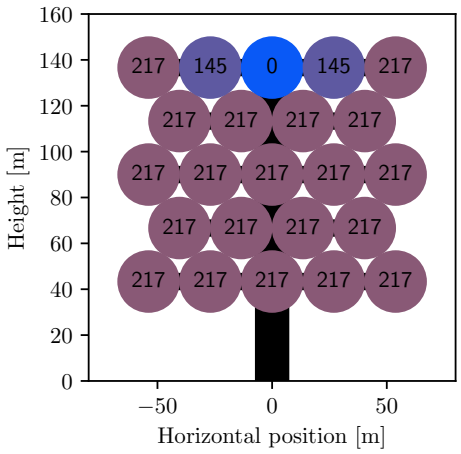

Figure 19. Power in kW for allocation with individual power and net bending moment constraints.

An interesting note to Fig. 20 is the presence of a thrust due to the surface area of the rotor, even though the rotor is not producing any power.

5.4 Net Yaw Moment Constraint

The final constraint considered is the net yaw moment constraint. Its importance might not be obvious, but one example might be the case where one rotor fails, after which the remaining rotors might produce an undesired net yaw moment. Including the constraint (17) in the optimization problem, one can easily compensate for failures by reducing the thrusts appropriately on the opposing side. Figure 21 and Fig. 22 show the powers and thrusts for a multi-rotor where rotor number 13 has suffered a failure and is not spinning. The example uses a wind velocity at the array center of 17 ms^{-1}. As found by the optimal control problem, the best thing to do is to reduce the thrust on the outer and uppermost rotor on the opposite side, rotor number 19. This way the smallest possible reduction of power, 7 %, is achieved, while at the same time reducing the bending moment to a minimum.

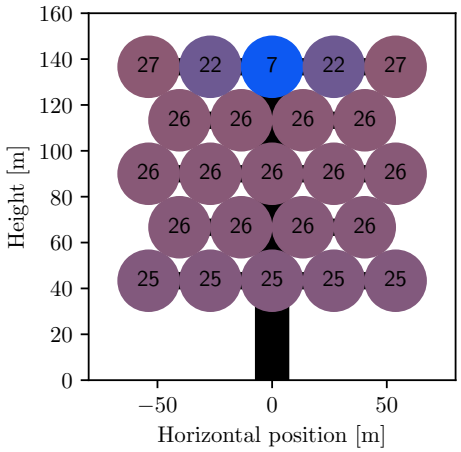

Figure 20. Thrusts in kN for allocation with individual power and net bending moment constraints.

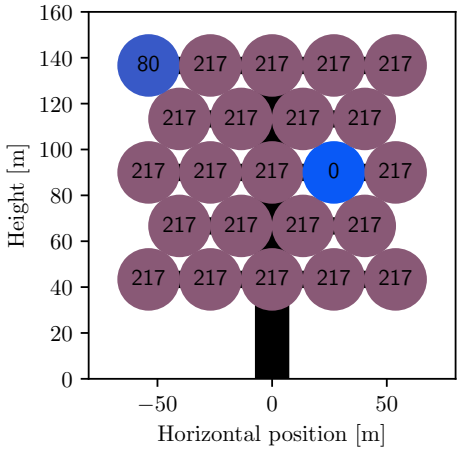

Figure 21. Powers in kW for allocation with individual power and net yaw moment constraints.

6 Multi-Rotor Wind Turbine Allocation Strategies

The control strategy for the general case presented in the optimization problem (14) through (18) can be too computationally complex to solve for practical real-time applications. This section will suggest some high level control schemes, utilizing multi-rotor properties that are predicted by the proposed model, that should be viable for real-time applications.

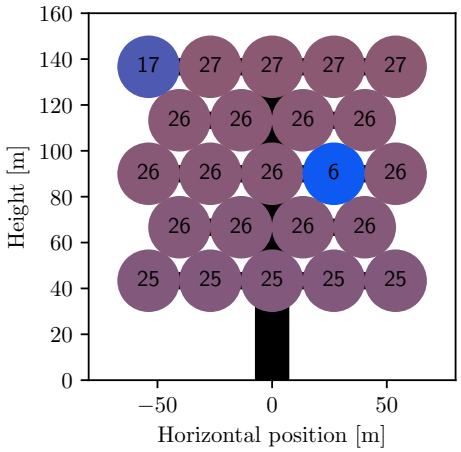

Figure 22. Thrusts in kN for allocation with individual power and net yaw moment constraints.

6.1 Scheduled Maximum Power Point Tracking

The DMPPT algorithm developed for the unconstrained case is not applicable when there are active constraints. Assuming that each rotor only is constrained by an individual power constraint, the DMPPT algorithm can be redesigned to respect this constraint by reducing the power once it reaches the rated power. The main issue with the redesigned controller is that the power constraint makes it not minimum phase Dalala et al. (2013). After the rotor reaches the rated power, the power is controlled by the generator torque which has to increase briefly, possibly exceeding the power constraint, to reduce the rotational rate sufficiently for the steady-state power to be lower, after which the generator can reduce its torque and power. Luckily, similar issues have been investigated and solved by Barzegar-Kalashani et al. (2023); Dalala et al. (2013), so it is believed that such a controller can be successfully designed and implemented.

In contrast to the DMPPT algorithm, the current approach makes the somewhat unconventional assumption of the net flow through the rotor being available either as a measurement or an estimate. The net flow is used as input to the control algorithm, that based on this returns the optimal rotational velocity of the rotor. A high-gain controller can then be used to control the system to follow this reference. This type of control scheme will be called the Scheduled Maximum Power Point Tracking (SMPPT) controller.

Figure 23 shows the optimal relation between the net flow through the rotor and the rotational velocity that maximizes the power until the power constraint is reached at around 7.5 ms^{-1}, after which the power is kept at the constraint. The SMPPT algorithm heavily relies on this relation, which has to be tuned to each physical system by formulating an accurate model and computing the optimal solutions numerically. With these results at hand, one can then model the relation using a neural network.

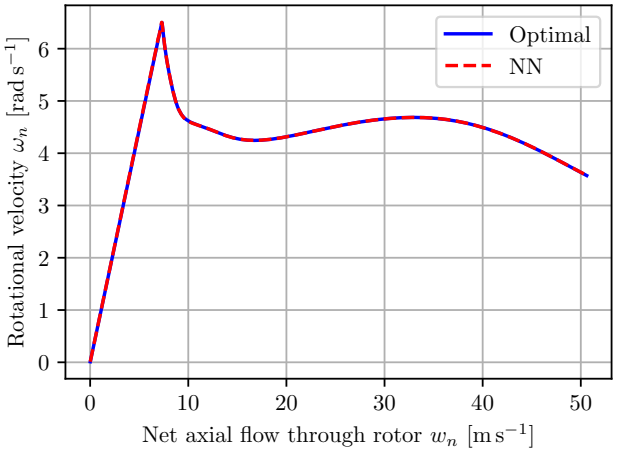

Figure 23. Optimal setpoints for rotational velocity and the fitted neural network (NN).

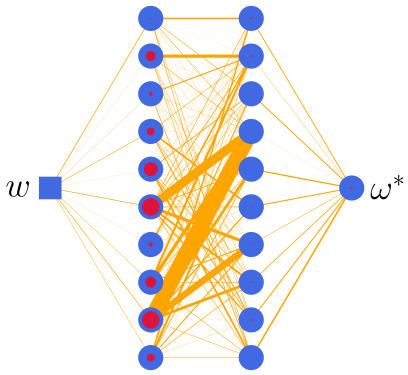

Figure 24. Neural network for SMPPT.

A neural network as shown in Fig. 24 was designed, implemented and trained to reproduce the relations from Fig. 23 for net axial flows from 0.01 ms^{-1} to 50 ms^{-1}. The same framework as for the airloads was used for implementation and training.

6.1.1 Thrust and Torque Schedule

290 An interesting feature arises when employing the SMPPT controller to the feedback model shown in Fig. 2: The airloads can be substituted for the optimal airloads which include the mechanics, since at steady-state the rotational velocities are instantly determined by the net flow. This gives a direct map from the net flow to the generated forces as shown in Fig. 25, simplifying the system block diagram to Fig. 26. Assuming a multi-rotor with many reasonably small rotors, one can still describe dynamic

cases with the optimal airloads simplification, because the dynamics are governed by the inflow as shown in Matras and Pedersen (2024).

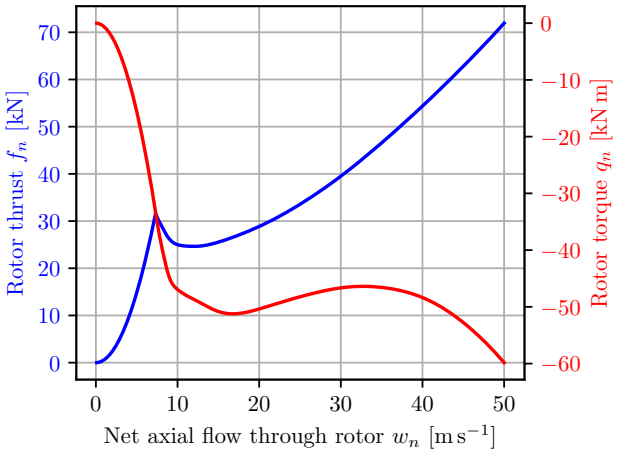

Figure 25. Thrust and torque schedules at steady state.

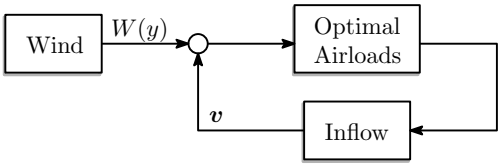

Figure 26. Block diagram with scheduling controller.

6.1.2 Restoring Moment

Similarly to the DMPPT, the SMPPT algorithm also generates a yaw moment when applied to a multi-rotor system that is not aligned with the freestream. In the unconstrained case the SMPPT is equivalent to the DMPPT where the restoring moment already has been shown. An example for the power constrained case with an ambient wind speed of 20 ms^{-1} at the array center, meaning that all turbines need to limit their power to comply with the constraint, is shown in Fig. 27. For modest misalignments, the expected restoring moment is present, but at large misalignments, the net yaw moment becomes destabilizing. The somewhat abrupt changes in the graph for the optimal solution are believed to be due to the different rows reaching the destabilizing misalignment at slightly different yaw misalignments.

Figure 28 shows the resulting net power as a function of the yaw misalignment. One can clearly see that by increasing the misalignment, one can effectively reduce the power. For single rotor systems this technique is known as furling, a term which will also be used for multi-rotors.

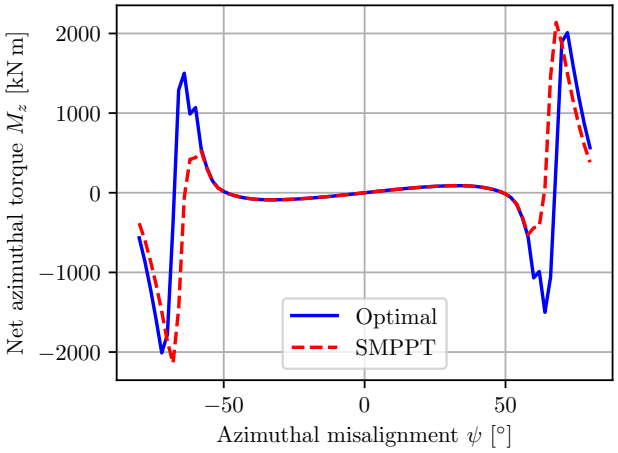

Figure 27. Influence of yaw misalignment on yaw moment when operating with power constraints.

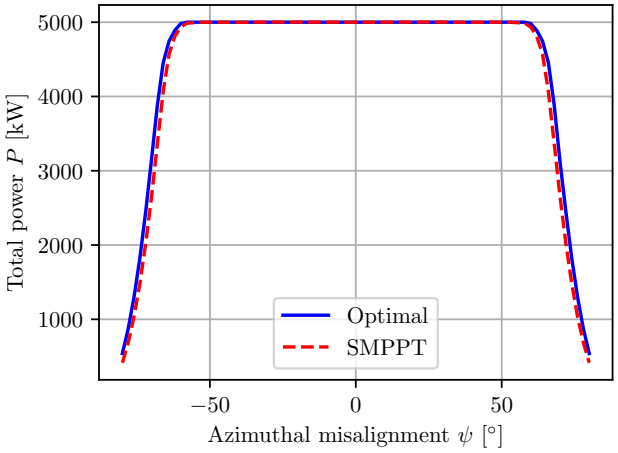

Figure 28. Influence of yaw misalignment on power when operating with power constraints.

An interesting observation in Fig. 27 and Fig. 28 is that the SMPPT controller performs identically in terms of power and net yaw moment to the numerically optimal solution of the multi-rotor problem for all main operating conditions. The major difference being that the SMPPT controller is almost trivial to compute. This highly simplifies the control, as one can employ the SMPPT controller, completely disregarding the interactions and still operate optimally as if one were to include the complex model with all interactions, at least in steady state with not too large yaw misalignments.

6.2 Furling Scheduled Maximum Power Point Tracking

The SMPPT algorithm presented in the previous section gives promising results in the individual power constrained case. In addition to constraining the power, it is often also desirable to minimize the structural loads. This can be achieved by utilizing furling, which not only reduces power, but also the thrust loading, as the axial component of the wind is reduced.

Consider the merged results from Fig. 27 and Fig. 28 as shown in Fig. 29. One can clearly see the blue dots marking the yaw misalignments that produce a zero yaw moment, while still producing maximum power. This is an advantageous equilibrium, even though it is unstable. The red dots mark the yaw misalignment where the power per bending moment is maximized, and it is of great interest that these points almost coincide with the unstable roots of the yaw moment.

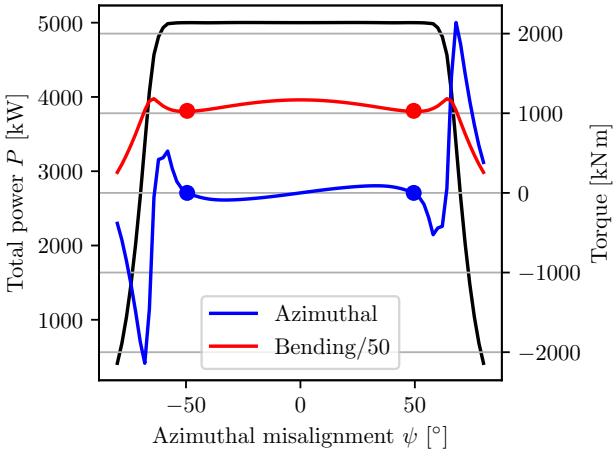

Figure 29. Slice of Fig. 30 at velocity 20 ms^{-1}.

Generalizing the results from Fig. 29 to a variety of velocities one can compute the yaw misalignment required to achieve zero yaw moment and maximum power per bending moment at any given velocity. The results of such an analysis are shown in Fig. 30, where also the case with no yaw misalignment is considered, the SMPPT algorithm. The blue line represents the line of zero yaw moment, while the red line the misalignment where the power per bending moment is maximized. It is clear that the zero net yaw moment misalignment almost coincides with the optimal solution where the power per bending moment is maximized for all freestream wind velocities!

Concluding the findings, one can approximate the optimal solution to the problem

$$\max_{\psi} \frac{P}{M_x} \quad \text{s.t. model equations} \tag{19}$$

by choosing the appropriate root of the yaw moment, namely the unstable equilibrium, rather than solving a complicated global numerical optimization problem. Furthermore, each individual multi-rotor wind turbine can still be decoupled using the SMPPT algorithm. The main challenge lies in keeping the multi-rotor at the unstable equilibrium, which can be done using a variety of techniques based on either differential thrusting or with some sort of yaw actuator.

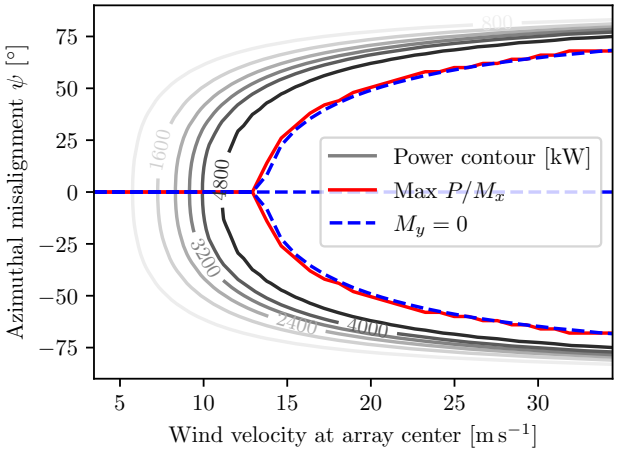

Figure 30. Optimal furling.

The SMPPT algorithm in cooperation with a global governor that ensures the operation at the optimal root of the net yaw moment curve is named the Global Governor Scheduled Maximum Power Point Tracking (GGSMPPT) algorithm. As in the unconstrained case, such a control strategy is a self-optimizing control scheme by definition of Skogestad and Postlethwaite (2005).

Based on simulations of other rotor layouts and counts, it is believed that the multi-rotor properties required for the GGSMPPT controller to work are a general phenomenon in multi-rotor wind turbines with at least one pair of vertically aligned and horizontally spaced rotors.

7 Discussion

Three control algorithms for the control of multi-rotor systems have been proposed:

- The general numerical optimization problem in (14).
- The SMPPT algorithm for the case with individual power constraints.
- The GGSMPPT which also reduces the net yaw loads by furling.

The yaw misalignment for the three control algorithms at steady state is shown in Fig. 31, and the corresponding power output is shown in Fig. 32. It is clear that all three algorithms perform identically in terms of power, but only the GGSMPPT algorithm approximates the optimal furling angle. One of the consequences of this is the difference in bending moments shown in Fig. 33. Both the numerically optimal solution and the GGSMPPT algorithms have the same, constant bending moment at high freestream wind velocities, while the SMPPT bending moment keeps increasing with wind speed because the multi-rotor remains aligned with the wind. These results show that furling could be a viable alternative to pitch control in

multi-rotor systems, and that the control system for such a design could be both computationally efficient and almost optimal by implementing the GGSMPPT controller.

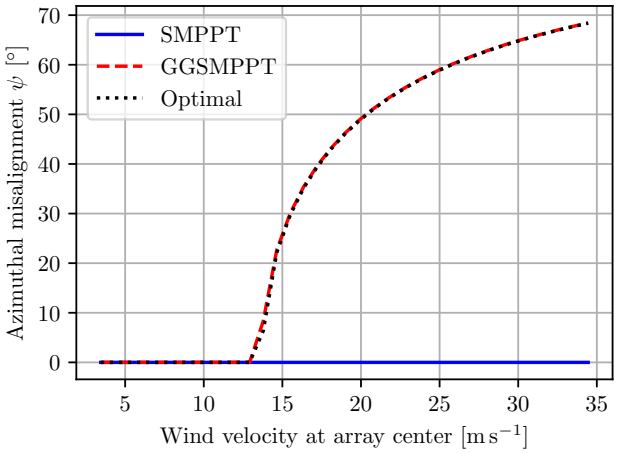

Figure 31. Yaw offset for various control algorithms.

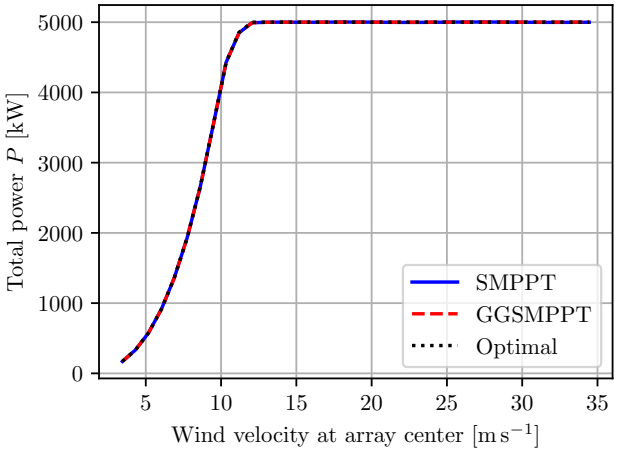

Figure 32. Power for various control algorithms.

The work presented here has been simplified under the stated assumptions, so it is not to be regarded as a complete analysis of the system. An effect mentioned in E. Muljadi (1998) which has not been included here considers the yaw moment generated on a single rotor when furling, in addition to the increase in flap loads and possibly increased noise. However, the smaller, potentially more rigid, multi-rotor blades might not be influenced as much by these effects as large rotor blades. Other aspects, such as how the furling shall be performed and its effects on the system have also not been investigated. Traditionally, furling

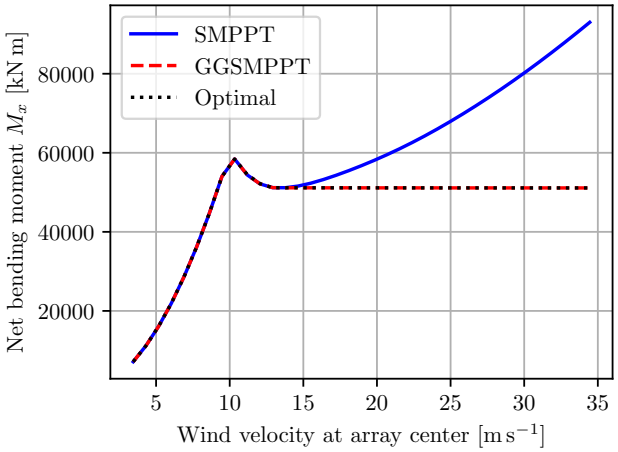

Figure 33. Bending moments about the bottom of the support.

has often been implemented with mechanical devices or actuators as discussed in Chirca et al. (2020), but these wear out over time. Using differential thrusting, one could potentially eliminate these issues, possibly at the cost of slightly reducing overall power production.

8 Conclusions

This paper has presented the novel steady-state multi-rotor wind turbine model and the high level control strategies presented in Matras (2025). The novelty of the model stems from the inclusion of, an admittedly somewhat simplified version of, the aerodynamic interactions between the rotors. These interactions predict some interesting phenomena for multi-rotor wind turbines, which as shown, can be leveraged to obtain simple high level control schemes that allow the use of a decoupled control strategy on the single-rotor level. The solution to the complex optimization problem involving numerous rotors and states can thus be approximated by an almost trivial algorithm.

These intriguing results open up many new questions and engineering challenges. Maybe the most fundamental area for future work involves the validation of the multi-rotor interaction effect and increasing the model's fidelity to further investigate the topic of furling. An investigation of furling and how this effect best is achieved naturally follows, as well as dynamic considerations to establish stability and a baseline for control algorithms. Other consequences of furling such as support structure and blade designs would also benefit from scientific attention.

Author contributions. Dr. Pedersen developed the models in collaboration with Dr. Matras, who also implemented, simulated and described the results and wrote the paper including all figures. Dr. Pedersen contributed as a supervisor during the whole process.

Competing interests. The authors declare that they have no conflict of interest.

References

Abdullah, M., Yatim, A., Tan, C., and Saidur, R.: A review of maximum power point tracking algorithms for wind energy systems, Renewable and Sustainable Energy Reviews, 16, 3220–3227, https://doi.org/https://doi.org/10.1016/j.rser.2012.02.016, 2012.

Apata, O. and Oyedokun, D.: An overview of control techniques for wind turbine systems, Scientific African, 10, e00 566, https://doi.org/10.1016/j.sciaf.2020.e00566, 2020.

Barzegar-Kalashani, M., Seyedmahmoudian, M., Mekhilef, S., Stojcevski, A., and Horan, B.: Small-scale wind turbine control in high-speed wind conditions: A review, Sustainable Energy Technologies and Assessments, 60, 103 577, https://doi.org/https://doi.org/10.1016/j.seta.2023.103577, 2023.

Bezanson, J., Edelman, A., Karpinski, S., and Shah, V. B.: Julia: A fresh approach to numerical computing, SIAM Review, 59, 65–98, https://doi.org/10.1137/141000671, 2017.

Chirca, M., Dranca, M., Oprea, C. A., Teodosescu, P.-D., Pacuraru, A. M., Neamtu, C., and Breban, S.: Electronically Controlled Actuators for a Micro Wind Turbine Furling Mechanism, Energies, 13, https://doi.org/10.3390/en13164207, 2020.

Dalala, Z. M., Zahid, Z. U., and Lai, J.-S.: New Overall Control Strategy for Small-Scale WECS in MPPT and Stall Regions With Mode Transfer Control, IEEE Transactions on Energy Conversion, 28, 1082–1092, https://doi.org/10.1109/TEC.2013.2287212, 2013.

Dunning, I., Huchette, J., and Lubin, M.: JuMP: A Modeling Language for Mathematical Optimization, SIAM Review, 59, 295–320, https://doi.org/10.1137/15M1020575, 2017.

E. Muljadi, T. Forsyth, C. P. B.: Soft-Stall Control versus Furling Control for Small Wind Turbine Power Regulation, windpower '98 ; Conference date: 27-04-1998 Through 01-05-1998, 1998.

Guenoune, I., Plestan, F., and Chermitti, A.: Control of a new structure of twin wind turbine, in: 2016 IEEE International Conference on Renewable Energy Research and Applications (ICRERA), pp. 490–495, https://doi.org/10.1109/ICRERA.2016.7884385, 2016.

Innes, M.: Flux: Elegant Machine Learning with Julia, Journal of Open Source Software, https://doi.org/10.21105/joss.00602, 2018.

Innes, M., Saba, E., Fischer, K., Gandhi, D., Rudilosso, M. C., Joy, N. M., Karmali, T., Pal, A., and Shah, V.: Fashionable Modelling with Flux, CoRR, abs/1811.01457, https://arxiv.org/abs/1811.01457, 2018.

Jamieson, P.: Innovation in wind turbine design, Wiley, Chichester, West Sussex ; Hoboken, N.J, 1st ed edn., ISBN 978-0-470-69981-2, oCLC: ocn719429298, 2011.

Jamieson, P. and Branney, M.: Structural Considerations of a 20MW Multi-Rotor Wind Energy System, Journal of Physics: Conference Series, 555, 012 013, https://doi.org/10.1088/1742-6596/555/1/012013, 2014.

Joglekar, M. and Loewy, R.: An Actuator-disc analysis of helicopter wake geometry and the corresponding blade response, USAAVLABS Technical Report 96-66, U.S.ARMY Air Mobility Research and Development Laboratory, 1970.

Johnson, K., Pao, L., Balas, M., and Fingersh, L.: Control of variable-speed wind turbines: Standard and adaptive techniques for maximizing energy capture, Control Systems, IEEE, 26, 70 – 81, https://doi.org/10.1109/MCS.2006.1636311, 2006.

Johnson, W.: Helicopter Theory, Dover Books on Aeronautical Engineering Series, Dover Publications, ISBN 9780486682303, https://books.google.cv/books?id=SgZheyNeXJIC, 1994.

Jonkman, J., Butterfield, S., Musial, W., and Scott, G.: Definition of a 5MW Reference Wind Turbine for Offshore System Development, Tech. rep., National Renewable Energy Laboratory (NREL), https://doi.org/10.2172/947422, 2009.

MacMahon, E. and Leithead, W.: Performance Comparison of Optimised and Non-Optimised Yaw Control for a Multi Rotor System, in: 2018 IEEE Conference on Control Technology and Applications (CCTA), pp. 1638–1643, IEEE, Copenhagen, ISBN 978-1-5386-7698-1, https://doi.org/10.1109/CCTA.2018.8511353, 2018.

Manwell, J. F., McGowan, J. G., and Rogers, A. L.: Wind Energy Explained: Theory, Design and Application, Wiley, Chichester, U.K, 2nd edition. edn., ISBN 9780470015001, 2010.

Matras, F.: Modeling, Simulation and Control of Multirotor Systems, Ph.D. thesis, Norwegian University of Science and Technology, 2025.

Matras, F. and Pedersen, M. D.: On the Necessity of Dynamic Inflow, Modeling, Identification and Control, 45, 29–39, https://doi.org/10.4173/mic.2024.1.3, 2024.

Matras, F., Reinhardt, D. P., Gryte, K., and Dinhoff Pedersen, M.: Homogeneous Parametric Modeling of Airloads, SYSTEM THEORY, CONTROL AND COMPUTING JOURNAL, 3, 1–11, https://doi.org/10.52846/stccj.2023.3.1.44, 2023.

Matras, F., Årsandøy, F. X. N., and Pedersen, M. D.: Modeling, Analysis and Optimization of Multirotor Power Consumption, in: 2024 10th International Conference on Control, Decision and Information Technologies (CoDIT), pp. 2680–2685, https://doi.org/10.1109/CoDIT62066.2024.10708188, 2024.

McTavish, S., Rodrigue, S., Feszty, D., and Nitzsche, F.: An investigation of in-field blockage effects in closely spaced lateral wind farm configurations, Wind Energy, 18, 1989–2011, https://doi.org/https://doi.org/10.1002/we.1806, 2015.

Myriad Wind Energy Systems: Developing modular wind energy for a more affordable and sustainable future, https://www.myriadwind.com/, 2024.

Sandhu, N.: Performance and Economic Analysis of Multi-Rotor Wind Turbine, EMITTER International Journal of Engineering Technology, 6, 289, https://doi.org/10.24003/emitter.v6i2.298, 2018.

Schlichting, H. and Shapiro, A. H.: Boundary Layer Theory, Sixth Edition, Journal of Applied Mechanics, 35, 846–846, https://doi.org/10.1115/1.3601336, 1968.

Skogestad, S. and Postlethwaite, I.: Multivariable feedback control : analysis and design, 2005.

Spagnolo, F., Papageorgiou, D., Galeazzi, R., Thomsen, J. S., and Sørensen, K. H.: Extremum Seeking Control for Multi-Rotor Wind Turbine in the Full-Load Region, IFAC-PapersOnLine, 53, 5386–5391, https://doi.org/10.1016/j.ifacol.2020.12.1525, 2020.

Sørensen, K. H., Knudsen, T., Filsoof, O. T., Hovgaard, T. G., Grunnet, J. D., Neto, J. X. V., and Wisniewski, R.: Multi-Rotor Wind Turbine Control Challenge - A Benchmark for Advanced Control Development, in: 2018 IEEE Conference on Control Technology and Applications (CCTA), pp. 1615–1622, IEEE, Copenhagen, ISBN 978-1-5386-7698-1, https://doi.org/10.1109/CCTA.2018.8511511, 2018.

van der Laan, M. P., Andersen, S. J., Ramos García, N., Angelou, N., Pirrung, G. R., Ott, S., Sjöholm, M., Sørensen, K. H., Vianna Neto, J. X., Kelly, M., Mikkelsen, T. K., and Larsen, G. C.: Power curve and wake analyses of the Vestas multi-rotor demonstrator, Wind Energy Science, 4, 251–271, https://doi.org/10.5194/wes-4-251-2019, 2019.

Wächter, A. and Biegler, L. T.: On the implementation of an interior-point filter line-search algorithm for large-scale nonlinear programming, Mathematical Programming, 106, 25–57, 2006.

Wind Catching Systems AS: Designed for floating wind, https://windcatching.com/, 2021.

Zhuang, J., Tang, T., Ding, Y., Tatikonda, S., Dvornek, N., Papademetris, X., and Duncan, J. S.: AdaBelief Optimizer: Adapting Stepsizes by the Belief in Observed Gradients, 2020.